Continuous Device Positioning and Synchronization in 5G Dense Networks with Skewed Clocks

Mike Koivisto*, Aki Hakkarainen*, Mário Costa†, Kari Leppänen†, and Mikko Valkama*
* Laboratory of Electronics and Communications Engineering, Tampere University of Technology, Finland
Emails: {mike.koivisto, aki.hakkarainen, mikko.e.valkama}@tut.fi
† Huawei Technologies Oy (Finland) Co., Ltd, Finland R&D Center
Emails: {mariocosta, kari.leppanen}@huawei.com

***Abstract*—Fifth generation (5G) radio networks are expected to provide remarkable improvements in the user experience due to faster data rates and lower latencies, for example. These kind of enhancements are made possible by several technical advances when compared to the existing networks. In particular, densification of network, device-centric network topology and exploitation of smart antennas, among others, will play key roles in network developments. In addition to obvious benefits in solely communications type of services, the aforementioned technological advances allow for completely new kind of applications. In this paper, we focus on user equipment (UE) positioning, and additionally show how also successful network synchronization can be done in 5G networks in a highly sophisticated, but low-complex network-centric solution. We will extend the analysis available in the existing literature to fully unsynchronized networks where the UEs as well as the network remote radio heads (RRHs) have clock offsets and skews with respect to a given reference clock. Our numerical performance analysis, based on realistic network and propagation models, show that the proposed method can provide sub-meter range positioning accuracy and highly accurate synchronization of the network elements.**

***Index Terms*—5G Networks, Extended Kalman Filter, Positioning, Synchronization, Ultra-dense Networks**

I. Introduction

Future fifth generation (5G) radio networks will provide tremendous enhancements compared to the existing mobile networks in terms of high data rates, overall capacity, and number of connected devices including vast amount of various sensors and Internet-of-Things (IoT) devices, for example [1], [2]. Despite the early stage of the 5G standardization process, it has already been envisioned that positioning will play an important role in future communication solutions. In the existing mobile communications networks, positioning has been only an add-on feature, whereas in 5G, it will not only enable vast amount of numerous location-based applications and services, like autonomous vehicles and intelligent transportation system (ITS), but also enhance the overall performance of the communication system itself, e.g., in terms of location-aware communication solutions like proactive radio resource management (RRM) [3]–[5]. In general, it is commonly expected among different bodies that 5G networks should be able to provide $1\,\mathrm{m}$ positioning accuracy for all indoor and outdoor terminals [1], [4], [6], [7] or even $10\text{-}30\,\mathrm{cm}$ for the most demanding use cases such as automotive applications [8], if designed properly. Such an envisioned accuracy is clearly outperforming the existing positioning techniques, e.g., observed time difference of arrivals (OTDoAs) in LTE where positioning accuracy is around few tens of meters [9] as well as GPS and WiFi fingerprinting based solutions where positioning accuracy is around $2\text{-}5\,\mathrm{m}$ [10], [11].

In particular, 5G networks will provide a convenient environment for positioning. In order to meet the demanding capacity and data-rate requirements of future 5G, network nodes will be most likely deployed with a high spatial density, thus increasing the probability of user equipment (UE) to be in line-of-sight (LoS) condition towards several network nodes at a time. Such a LoS condition together with the envisioned large bandwidths will also enable highly accurate time of arrival (ToA) estimation at the network nodes, later referred to as remote radio heads (RRHs), equipped with base band units (BBUs). In addition to ToAs, it is widely expected that smart antenna solutions such as antenna arrays will be exploited in the RRHs, thus enabling also highly accurate direction of arrival (DoA) estimation at the RRHs. These aforementioned estimates can be, in turn, fused for UE positioning and network synchronization in a network-centric manner by utilizing uplink (UL) pilot signals, which are anyway communicated between the UEs and RRHs for necessary channel estimation and scheduling purposes in time division duplex (TDD) networks. In contrast to the network-centric approach, positioning can be also carried out within a device but the cost is an increase in device energy consumption.

In this paper, a joint network-centric positioning and synchronization method for unsynchronized 5G ultra-dense network (UDN) is proposed. This paper is an extension of the work in [12] to the case where the access nodes (ANs) comprising the UDN are now allowed to have clock skews. In the first phase of the proposed method, DoAs and ToAs are tracked at LoS-RRHs using an extended Kalman filter (EKF)-based solution similar to that in [12]. Thereafter, the obtained DoA and ToA estimates are fused into UEs' location estimates as well as clock offsets and skews of both UEs and RRHs in the second EKF-based processing stage, which can be thereafter used to synchronize UEs and RRHs within the network. In the existing literature, joint positioning and synchronization is explored in the case of unsynchronized UEs and synchronized or phase-locked network elements, e.g., in [12], [13], whereas joint positioning and synchronization methods, where the network elements have skews in their clocks, have not been widely

This work was supported by the Doctoral Program of the President of Tampere University of Technology, the Finnish Funding Agency for Technology and Innovation (Tekes), under the projects "5G Networks and Device Positioning", "TAKE-5", and "Future Small-Cell Networks using Reconfigurable Antennas".

considered in the existing literature.

The rest of the paper is organized as follows. First, general assumptions about the considered network and system are described in Section II. In Section III, the well-known equations of the generic EKF are shortly reviewed, while the equations and necessary models are then extended to cover the considered positioning and network synchronization scenarios in Sections III-B and III-C. Then, the performance of the proposed approach is evaluated using extensive simulations and numerical evaluations, and the obtained results are discussed and analyzed in Section IV. Finally, conclusions are drawn in Section V.

II. System Model

A. Network Architecture and Positioning Engine

In this paper, a centralized network architecture, where densely deployed RRHs are equipped with BBUs, is considered. In such an architecture, UDNs are deployed by attaching the RRHs to lamp posts below rooftops as illustrated in Fig. 1, and the exact locations of the RRHs are assumed to be known. Within the RRHs, cylindrical antenna arrays consisting of 10 dual-polarized cross-dipole elements are employed, thus allowing for DoA estimation in both azimuth and elevation directions. In addition to the BBUs, more demanding centralized processing such as scheduling and data fusion are taking place in a central unit of the network.

In the considered system, UEs periodically transmit UL pilot signals employing orthogonal frequency-division multiplexing (OFDM) waveforms in an orthogonal frequency-division multiple access (OFDMA) manner in a multiuser network. These UL signals allow for continuous network-centric positioning solutions since such pilots are anyway transmitted from the UEs to the RRHs in order to obtain necessary channel estimates at the transmitter for scheduling purposes. Each of the receiving RRHs first determines whether or not it is in LoS condition towards a given UE based on, e.g., Rice-factor which is typically around 10-20 dB in UDNs [14]. In addition to channel estimation, these UL pilot signals can be then also utilized for DoA and ToA estimation at an individual LoS-RRH. In the considered solution, these temporal and spatial estimates are, thereafter, communicated to a central entity of a network where the actual UE positioning and network synchronization procedure is carried out by fusing the estimated DoA and ToA measurements from all LoS-RRHs into UE location estimates as well as UE and LoS-RRHs clock parameter estimates.

B. Clock Model

In order to model the unsynchronized clocks within a network, the following clock model for a time-varying clock offset with a skew is assumed, and it stems from the work in [15]

$$\rho[k] = \rho[k-1] + \Delta t \alpha[k-1] \tag{1}$$
$$\alpha[k] = \beta\alpha[k-1] + v[k], \tag{2}$$

where the constant parameter $|\beta| < 1$, as well as $\rho[k]$ and $\alpha[k]$ denote clock offset and skew at the time-instant k, respectively. Furthermore, Δt denotes a time interval between the consecutive time-instants $k-1$ and k, and $v[k] \sim \mathcal{N}(0, \sigma_\eta^2)$ is a driving noise of the clock skew. For the sake of simplicity, the clock offsets at UEs and RRHs are assumed to follow the aforementioned models (1) and (2) in a way that the clock skews are assumed to be constant over time. Such an assumption typically holds for stable clock oscillators and in relatively ideal environments where, e.g., the temperature is not significantly varying over the time of interest. Similar simplifications have been made, e.g., in [16], [17], where stand-alone clock parameter estimation and tracking is carried out. Moreover, based on the obtained measurements in [15], the average clock skew over a long time period can indeed be considered constant in a temperature controlled environment.

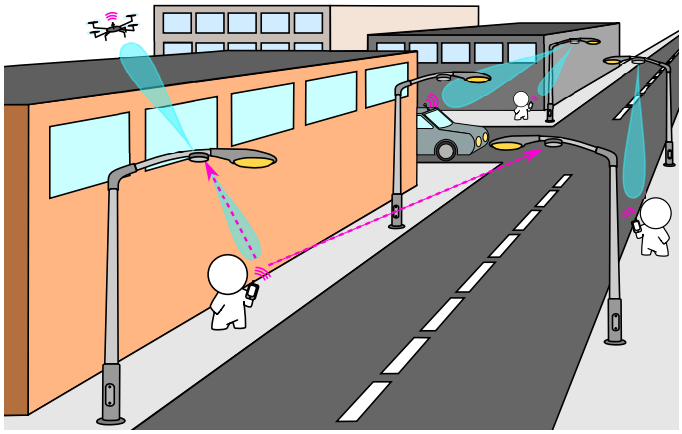

Fig. 1. In the considered 5G UDN, the RRHs are attached to lamp posts, and UEs transmit periodical UL pilots towards the RRHs. These periodic UL pilot signals can be utilized also for continuous network-centric positioning.

C. Channel Model

In this paper, the following UL single-input-multiple-output (SIMO) multiantenna-multicarrier channel response model for $\mathcal{M}_{\text{AN}}$ receiving antenna elements and OFDM waveforms with $\mathcal{M}_f$ active subcarriers is exploited [12], [18]

$$\hat{\mathbf{g}}_{\ell_i} \approx \mathbf{B}_{\ell_k}(\theta, \varphi, \tau)\boldsymbol{\gamma} + \mathbf{n}, \tag{3}$$

where $\hat{\mathbf{g}}_{\ell_i} \in \mathbb{C}^{\mathcal{M}_{\text{AN}}\mathcal{M}_f \times 1}$ is a channel response vector estimated at the RRH with an index ℓ_i. Furthermore, $\mathbf{B}_{\ell_i}(\theta, \varphi, \tau) \in \mathbb{C}^{\mathcal{M}_{\text{AN}}\mathcal{M}_f \times 2}$ denotes the polarimetric response of the ℓ_i^{th} multi-antenna RRH whereas $\boldsymbol{\gamma} \in \mathbb{C}^{2\times 1}$ denotes complex path weights. Moreover, $\mathbf{n} \in \mathbb{C}^{\mathcal{M}_{\text{AN}}\mathcal{M}_f \times 1}$ in (3) denotes a complex-circular zero-mean Gaussian noise with variance σ_n^2. In particular, the polarimetric antenna array response $\mathbf{B}_{\ell_i}(\theta, \varphi, \tau)$ is given in terms of the effective aperture distribution function (EADF) [18] as

$$\begin{aligned}\mathbf{B}_{\ell_i}(\theta, \varphi, \tau) = [&\mathbf{G}_H \mathbf{d}(\varphi, \theta) \otimes \mathbf{G}_f \mathbf{d}(\tau), \\ &\mathbf{G}_V \mathbf{d}(\varphi, \theta) \otimes \mathbf{G}_f \mathbf{d}(\tau)],\end{aligned} \tag{4}$$

where $\otimes$ denotes the Kronecker product, and $\mathbf{G}_H \in \mathbb{C}^{\mathcal{M}_{\text{AN}} \times \mathcal{M}_a \mathcal{M}_e}$ is the EADF for horizontal excitation and similarly $\mathbf{G}_V \in \mathbb{C}^{\mathcal{M}_{\text{AN}} \times \mathcal{M}_a \mathcal{M}_e}$ is the EADF for vertical excitation. Numbers of the determined array response modes in EADF for azimuth and elevation are denoted as $\mathcal{M}_a$ and $\mathcal{M}_e$, respectively. The array calibration data, represented using the aforementioned EADFs, can be determined in well-defined propagation environments, e.g., in an anechoic chamber [18]. Furthermore, $\mathbf{G}_f \in \mathbb{C}^{\mathcal{M}_f \times \mathcal{M}_f}$ in (4) denotes the frequency response of the RRH receivers, and $\mathbf{d}(\varphi, \theta) \in \mathbb{C}^{\mathcal{M}_a \mathcal{M}_e}$ is written as

$$\mathbf{d}(\varphi, \theta) = \mathbf{d}(\theta) \otimes \mathbf{d}(\varphi), \tag{5}$$

where $\mathbf{d}(\varphi) \in \mathbb{C}^{\mathcal{M}_a}$ and $\mathbf{d}(\theta) \in \mathbb{C}^{\mathcal{M}_e}$ as well as $\mathbf{d}(\tau) \in \mathbb{C}^{\mathcal{M}_f}$ in (4) are Vandermonde structured vectors. These vectors map the spatial and delay parameters to the corresponding frequency domain such that

$$\mathbf{d}(\tau) = \left[e^{-j\pi(\mathcal{M}_f-1)f_0\tau}, \ldots, 1, \ldots, e^{j\pi(\mathcal{M}_f-1)f_0\tau}\right]^{\mathrm{T}}. \quad (6)$$

The corresponding directional vectors $\mathbf{d}(\varphi)$ and $\mathbf{d}(\theta)$ can be formulated similarly using the relation $\varphi/2 = \pi f_0 \tau$, where f_0 denotes the subcarrier spacing of the employed OFDM waveform. Throughout this paper, the EADFs are assumed to be known for all RRHs.

It is important to note that the somewhat simple models described in this section are exploited by the DoA and ToA estimation, and the tracking algorithm described in Section III-B, but are not employed for simulating the channel between the UE and RRHs. For generating the underlying multipath radio channel between a UE and RRHs, an extensive ray-tracing tool is employed [14], as described in more detail in Section IV. Note also that the model in (3) may be time-varying, including the complex-valued path-weights. This is exploited by the proposed tracking algorithm described in Section III-B.

III. Proposed Positioning and Synchronization Solution

A. Extended Kalman filter (EKF)

In order to sequentially estimate the state of a desired system, an EKF-based sequential estimation method, where non-linear models are linearized using first-order Taylor approximations, is employed in this paper [19]. Let us consider the following linear state transition and non-linear measurement models for a system

$$\mathbf{s}[k] = \mathbf{F}[k]\mathbf{s}[k-1] + \mathbf{w}[k] \quad (7)$$

$$\mathbf{y}[k] = \mathbf{h}(\mathbf{s}[k]) + \mathbf{v}[k], \quad (8)$$

where $\mathbf{s}[k] \in \mathbb{R}^n$ and $\mathbf{y}[k] \in \mathbb{R}^m$ are state and measurement vectors at a time instant k, respectively. Moreover, $\mathbf{F}[k] \in \mathbb{R}^{n\times n}$ is a state transition matrix and $\mathbf{h} : \mathbb{R}^n \rightarrow \mathbb{R}^m$ is a non-linear measurement model function. Finally, $\mathbf{w}[k] \sim \mathcal{N}(0, \mathbf{Q}[k])$ and $\mathbf{v}[k] \sim \mathcal{N}(0, \mathbf{R}[k])$ denote state and measurement model noise processes in the system. Let us further denote the *a priori* estimates as $\hat{\mathbf{s}}^-$ and $\hat{\mathbf{P}}^-$, and similarly the *a posteriori* estimates as $\hat{\mathbf{s}}^+$ and $\hat{\mathbf{P}}^+$. Using this notation and assuming the general models in (7) and (8), the *a posteriori* estimates at time step k can be obtained in the EKF as

$$\hat{\mathbf{s}}^-[k] = \mathbf{F}[k]\hat{\mathbf{s}}^+[k-1] \quad (9)$$

$$\hat{\mathbf{P}}^-[k] = \mathbf{F}[k]\hat{\mathbf{P}}^+[k-1]\mathbf{F}^{\mathrm{T}}[k] + \mathbf{Q}[k] \quad (10)$$

$$\mathbf{K}[k] = \hat{\mathbf{P}}^-[k]\mathbf{H}^{\mathrm{T}}[k](\mathbf{H}[k]\hat{\mathbf{P}}^-[k]\mathbf{H}^{\mathrm{T}}[k] + \mathbf{R}[k])^{-1} \quad (11)$$

$$\hat{\mathbf{s}}^+[k] = \hat{\mathbf{s}}^-[k] + \mathbf{K}[k]\left[\mathbf{y}[k] - \mathbf{h}(\hat{\mathbf{s}}^-[k])\right] \quad (12)$$

$$\hat{\mathbf{P}}^+[k] = (\mathbf{I} - \mathbf{K}[k]\mathbf{H}[k])\,\hat{\mathbf{P}}^-[k], \quad (13)$$

where $\mathbf{H}[k]$ is the Jacobian matrix of the non-linear measurement model function $\mathbf{h}$ in (8), evaluated at $\hat{\mathbf{s}}^-[k]$. Note that the aforementioned equations are only employed in the positioning and synchronization EKF whereas a more convenient formulation of the EKF is employed for tracking the DoAs and ToAs.

B. DoA and ToA Estimation and Tracking EKF

As described earlier in this paper, the periodically transmitted UL pilots can be also utilized for DoA and ToA estimation as well as tracking at each LoS-RRH. In this paper, we exploit the efficient and computationally appealing EKF-based solution proposed in our earlier work [12] for tracking the DoAs and ToAs. In particular, such an EKF is based on the model in (3) and exploits the obtained channel estimates. In contrast to the Kalman gain form of the EKF described in Section III-A, the information form of the EKF is applied for tracking the DoA and ToA since it is computationally more efficient than the former whenever the dimension of the state vector is smaller than that of the measurement vector. The tracked DoA and ToA are then exploited by the positioning and synchronization EKF described in Section III-C.

Note that the EKF described in this section for tracking the DoA and ToA of the LoS path *does not* assume the complex-valued path-weights to be known. In particular, we consider such path-weights nuisance parameters, and employ a so-called concentrated log-likelihood function in order to decouple the DoA and ToA from the path-weights; see [12] for details.

C. Proposed Positioning and Synchronization EKF

In order to fuse the obtained DoA and ToA estimates into UE's location as well as UE's and LoS-RRHs' clock parameter estimates, a second EKF stage for positioning and synchronization is employed in a central entity of the network. In addition to UE's location and velocity, also clock offsets and skews of the UE and LoS-RRHs are estimated and tracked jointly within this EKF. This is an extension of the work in [12] since therein the ANs were considered to have zero clock-skews.

Let us denote a set of LoS-RRH indices at time instant k as $\mathcal{S}_k$, and let us further assume that UEs are following a nearly constant velocity model while the clocks of the UEs and RRHs evolve according to (1) and (2). Hence, the state of the system can be written as

$$\mathbf{s}[k] = \left[\mathbf{s}_{\mathrm{UE}}^{\mathrm{T}}[k], \mathbf{s}_{\ell_1}^{\mathrm{T}}[k], \ldots, \mathbf{s}_{\ell_{N_k}}^{\mathrm{T}}[k]\right]^{\mathrm{T}}, \quad (14)$$

where N_k is the cardinality of the set $\mathcal{S}_k$, i.e., denotes the number of LoS-RRHs at the time instant k. Moreover, the state of a single UE $\mathbf{s}_{\mathrm{UE}}[k]$ and i^{th} LoS-RRH $\mathbf{s}_{\ell_i}[k]$ in (14) can be written as

$$\mathbf{s}_{\mathrm{UE}}[k] = [x[k], y[k], z[k], v_x[k], v_y[k], v_z[k], \rho[k], \alpha[k]]^{\mathrm{T}} \quad (15)$$

$$\mathbf{s}_{\ell_i}[k] = [\rho_{\ell_i}[k], \alpha_{\ell_i}[k]]^{\mathrm{T}}, \quad (16)$$

where $\ell_i \in \mathcal{S}_k, \forall i = 1, \ldots, N_k$. Furthermore, $[x[k], y[k], z[k]]^{\mathrm{T}}$ and $[v_x[k], v_y[k], v_z[k]]^{\mathrm{T}}$ are the 3D location and velocity of a given UE, respectively. Finally, $\rho[k]$ and $\alpha[k]$ denote the clock offset and skew of the UE, while $\rho_{\ell_i}[k]$ and $\alpha_{\ell_i}[k]$ denote the clock offset and skew of the i^{th} LoS-RRH $\ell_i \in \mathcal{S}_k$. For the sake of simplicity, it is assumed that all the clock offsets and skews are determined with respect to a reference RRH with a stable clock that has a nominal zero offset.

In the considered system, the state transition and measurement models can be expressed as in (7) and (8). Assuming the afore-

mentioned motion and clock models as well as the state in (14), the state transition matrix $\mathbf{F}[k]$ can be written as

$$\mathbf{F}[k] = \text{blkdiag}\left(\mathbf{F}_{\text{UE}}, \mathbf{F}_{\ell_1}, \ldots, \mathbf{F}_{\ell_{N_k}}\right), \tag{17}$$

where the matrices $\mathbf{F}_{\text{UE}} \in \mathbb{R}^{8\times 8}$ and $\mathbf{F}_{\ell_i} \in \mathbb{R}^{2\times 2}$, $\forall \ell_i \in \mathcal{S}_k$ are

$$\mathbf{F}_{\text{UE}} = \begin{bmatrix} \mathbf{I} & \Delta t\mathbf{I} & \mathbf{0} & \mathbf{0} \\ \mathbf{0} & \mathbf{I} & \mathbf{0} & \mathbf{0} \\ \mathbf{0} & \mathbf{0} & 1 & \Delta t \\ \mathbf{0} & \mathbf{0} & 0 & \beta \end{bmatrix}, \quad \mathbf{F}_{\ell_i} = \begin{bmatrix} 1 & \Delta t \\ 0 & \beta \end{bmatrix}, \tag{18}$$

where Δt denotes the time-interval between the consecutive time instants $k-1$ and k. In addition, the process noise covariance in the state model (7) can be similarly written as

$$\mathbf{Q}[k] = \text{blkdiag}\left(\mathbf{Q}_{\text{UE}}, \mathbf{Q}'_{\text{UE}}, \mathbf{Q}_{\ell_1}, \ldots, \mathbf{Q}_{\ell_{N_k}}\right), \tag{19}$$

where the sub-matrices $\mathbf{Q}_{\text{UE}} \in \mathbb{R}^{6\times 6}$, $\mathbf{Q}'_{\text{UE}} \in \mathbb{R}^{2\times 2}$, and $\mathbf{Q}_{\ell_i} \in \mathbb{R}^{2\times 2}$, $\forall \ell_i \in \mathcal{S}_k$, are

$$\mathbf{Q}_{\text{UE}} = \begin{bmatrix} \frac{\sigma_v^2 \Delta t^3 \mathbf{I}_{3\times 3}}{3} & \frac{\sigma_v^2 \Delta t^2 \mathbf{I}_{3\times 3}}{2} \\ \frac{\sigma_v^2 \Delta t^2 \mathbf{I}_{3\times 3}}{2} & \sigma_v^2 \Delta t \mathbf{I}_{3\times 3} \end{bmatrix} \tag{20}$$

$$\mathbf{Q}'_{\text{UE}} = \text{diag}([\sigma_\rho^2, \sigma_\alpha^2]), \quad \mathbf{Q}_{\ell_i} = \text{diag}([\sigma_{\rho_{\ell_i}}^2, \sigma_{\alpha_{\ell_i}}^2]). \tag{21}$$

Here, σ_v^2, σ_ρ^2, and σ_α^2 denote variances of the UE velocity, clock offset and skew, respectively, whereas $\sigma_{\alpha_{\ell_i}}^2$ and $\sigma_{\rho_{\ell_i}}^2$ denote variances of the ℓ_i^{th} RRH clock skew and offset respectively.

In a central entity of the network, the obtained DoAs and ToAs, denoted by $\mathbf{y}_{\ell_i}[k] = [\theta_{\ell_i}[k], \varphi_{\ell_i}[k], \tau_{\ell_i}[k]]^{\text{T}}$, and their corresponding covariance estimate, denoted by $\mathbf{R}_{\ell_i}[k]$, from individual LoS-RRHs are augmented into a single measurement vector $\mathbf{y}[k] = [\mathbf{y}_{\ell_1}[k], \ldots, \mathbf{y}_{\ell_{N_k}}[k]]^{\text{T}}$ and a measurement noise covariance matrix $\mathbf{R}[k] = \text{blkdiag}(\mathbf{R}_{\ell_1}[k], \ldots, \mathbf{R}_{\ell_{N_k}}[k])$. Thus, the measurement model function is $\mathbf{h}(\mathbf{s}[k]) = [\mathbf{h}_{\ell_1}(\mathbf{s}[k]), \ldots, \mathbf{h}_{\ell_{N_k}}(\mathbf{s}[k])]^{\text{T}}$, where

$$\mathbf{h}_{\ell_i}(\mathbf{s}[k]) = \begin{bmatrix} \arctan\left(\frac{\Delta y_{\ell_i}[k]}{\Delta x_{\ell_i}[k]}\right) \\ \arctan\left(\frac{\Delta z_{\ell_i}[k]}{\|\mathbf{p}[k]-\mathbf{p}_{\ell_i}\|_{\text{2D}}}\right) \\ \frac{\|\mathbf{p}[k]-\mathbf{p}_{\ell_i}\|_{\text{3D}}}{c} + (\rho_{\ell_i}[k] - \rho[k]) \end{bmatrix} \tag{22}$$

for all $\ell_i \in \mathcal{S}_k$. Here, Δx_{ℓ_i}, Δy_{ℓ_i}, and Δz_{ℓ_i} denote the distances between the i^{th} LoS-RRH and a given UE in x, y, and z directions, respectively. Finally, $\|\mathbf{p}[k] - \mathbf{p}_{\ell_i}\|_{\text{2D}}$ and $\|\mathbf{p}[k] - \mathbf{p}_{\ell_i}\|_{\text{3D}}$ denote the 2D and 3D distances between the same LoS-RRH and UE, while c is the speed of light.

IV. Numerical evaluations and analysis

A. Simulation setup

In order to demonstrate and evaluate the performance of the proposed positioning and synchronization EKF, referred to as DoA&ToA EKF, in terms of 3D positioning and clock parameter estimation accuracy, comprehensive numerical evaluations are carried out and the obtained results are then analyzed in this section. For the evaluations, the extensive METIS map-based ray-tracing channel model is implemented in the outdoor METIS Madrid map environment [20], using the uniform theory of diffraction (UTD) in order to model the propagation of received UL pilot signals [14] realistically. Furthermore, the transmit power of the tracked UEs is set to $10\,\text{dBm}$, and interfering UEs with the same transmit power are placed randomly $250\,\text{m}$ away from the UE with a density of $1000\,\text{interferers/km}^2$.

The considered 5G network is assumed to deploy OFDMA-based radio access with $240\,\text{kHz}$ subcarrier spacing and $5\,\text{MHz}$ reference signal bandwidth, for a single UE, comprising of 20 pilot subcarriers [21]. In addition, subframes of length $0.2\,\text{ms}$ containing 14 OFDM symbols are incorporated into the radio subframe structure. Moreover, UL pilot signals of the UEs within a specific RRH coordination area are assumed to be orthogonal through proper time and frequency scheduling. Furthermore, the DoAs and ToAs from 2 closest LoS-RRHs are utilized for positioning within the EKF every $100\,\text{ms}$. For comparison purposes, also an EKF-based solution, where constant offsets at the RRHs' clocks without skews are assumed while still considering a constant clock skew at a UE, is implemented in this paper.

In order to ensure convergence of the EKFs in the beginning, the initialization procedure proposed in [12] is carried out in the beginning of each random UE trajectory. These trajectories are generated using an empirical polynomial acceleration model, which allows for modeling the movement of a vehicle realistically in an urban environment [22], such that the velocity of a simulated vehicle is 20-$50\,\text{km/h}$. For both EKFs, similar numerology for initializing the model parameters, the reference clock parameters of the UEs and RRHs as well as the parameters within the EKF are used as in [23]. Since constant skews are assumed at UE and RRHs, the standard deviations (STDs) in (21) are set to extremely low values, i.e., $\sigma_\alpha = \sigma_{\alpha_{\ell_i}} = 10^{-13}$, and the STDs of the clock offsets are set to $\sigma_\rho = \sigma_{\rho_{\ell_i}} = 10^{-11}$.

B. Results

In order to assess the performance of the proposed DoA&ToA EKF, cumulative distribution functions (CDFs) of 3D positioning errors are depicted in Fig. 2 whereas CDFs of clock offset and skew errors for both UE and LoS-RRHs in the considered scenarios are illustrated in Figs. 3a and 3b, respectively. As expected, the positioning performance slightly degrades in the case where the clocks at RRHs are assumed to have skews. Interestingly, sub-meter positioning accuracy is achieved even in the case of more realistic clock scenario almost in 80% of situations. Such a probability for below $1\,\text{m}$ positioning accuracy in 5G is also envisioned, e.g., in [7]. In addition, in 90% of the cases, below $2\,\text{m}$ and $1.5\,\text{m}$ positioning performance can be reached when assuming constant skew and constant offset at RRHs' clocks, respectively.

Based on the obtained clock parameter estimation results in Figs. 3a and 3b, the clock offset and skew errors of a given UE and LoS-RRHs are smaller in the case where constant offsets at RRHs are assumed, as expected. In such a scenario, most of the variation in the clock offset estimates can be due to the UE, whereas more equal error weighting occurs when the more realistic clock model is assumed also at the RRHs. With the considered numerology, even below $10\,\text{ns}$ and $1\,\text{ns}$ estimation accuracies for the UE clock offsets and skews can be obtained with a probability of 99%, respectively. In the case of the more realistic clock model at RRHs, slightly worse performance is achieved due to more inaccurate clock skew estimation which in turn affects the clock offset and location estimation as well.

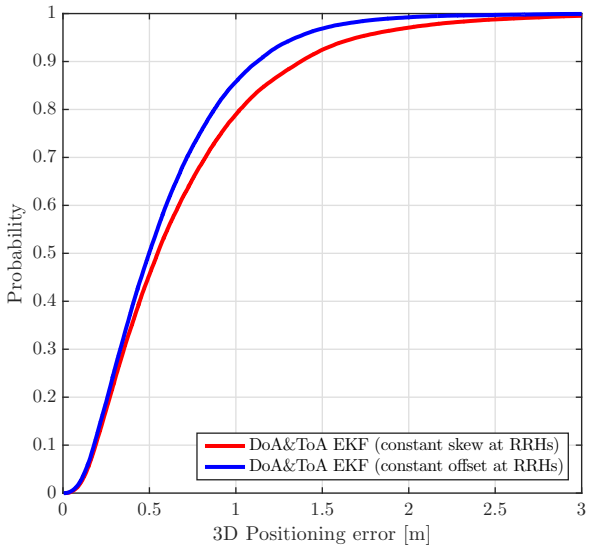

Fig. 2. CDFs of 3D positioning errors for both constant skew and constant offset scenarios.

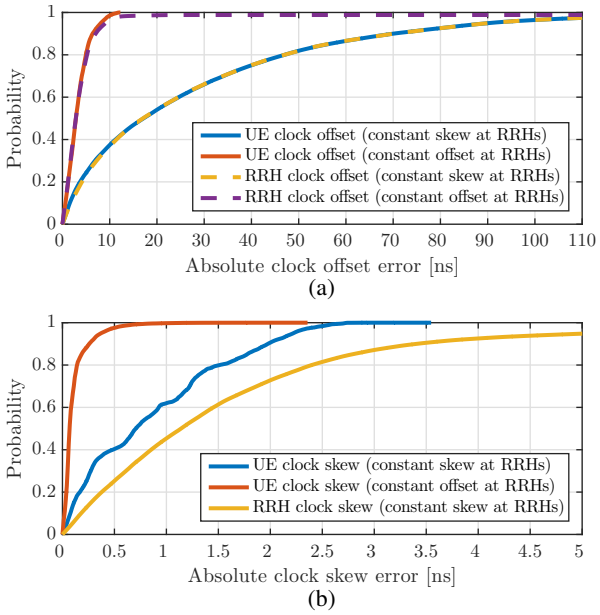

Fig. 3. Clock (a) offset and (b) skew errors for a UE and LoS-RRHs

Despite the slightly unfavourable clock offset estimation performance in the more demanding scenario, below 100 ns estimation accuracy can be reached. As a concrete example, in OTDoA-based positioning in LTE, the typical value for the clock offsets among the RRHs is assumed to be less than 100 ns [24, Table 8-1], whereas the expected timing misalignment requirement for future 5G small-cell networks is less than 500 ns [25], thus giving a somewhat concrete quantitative reference regarding network synchronization. Due to the imperfect clock parameter estimation performance, the clock offset and skew errors of the LoS-RRHs can eventually diverge after the connection to certain LoS-RRHs is lost. However, the proposed solution can be further extended to a multiuser scenario, thus providing continuous synchronization within a network through proper network time propagation.

V. Conclusion

In this paper, an EKF-based solution for joint device positioning and network synchronization under unsynchronized clocks with clock skews in 5G UDNs was proposed. Such a solution is able to provide continuous and computationally efficient positioning and synchronization in a network-centric manner without draining the battery of a device. Based on extensive simulations and numerical evaluations, the proposed solution was shown to provide sub-meter positioning accuracy even under realistic clock model assumptions with clock skews. As a valuable by-product, the proposed method is also able to estimate the clock parameters of a given device and LoS-RRHs with a relatively high accuracy.

References

[1] 5G Forum, "5G white paper: New wave towards future societies in the 2020s," Mar. 2015. [Online]. Available: http://www.5gforum.org/5GWhitePaper/5G_Forum_White_Paper_Service.pdf

[2] F. Boccardi, R. W. Heath, A. Lozano, T. L. Marzetta, and P. Popovski, "Five disruptive technology directions for 5G," *IEEE Commun. Mag.*, vol. 52, no. 2, pp. 74–80, Feb. 2014.

[3] S. Sand, A. Dammann, and C. Mensing, *Positioning in Wireless Communication Systems*, 1st ed. John Wiley & Sons Ltd., 2014.

[4] 5G-PPP, "5G empowering vertical industries," Feb. 2015. [Online]. Available: https://5g-ppp.eu/wp-content/uploads/2016/02/BROCHURE_5PPP_BAT2_PL.pdf

[5] R. Di Taranto, S. Muppirisetty, R. Raulefs, D. Slock, T. Svensson, and H. Wymeersch, "Location-aware communications for 5G networks: How location information can improve scalability, latency, and robustness of 5G," *IEEE Signal Process. Mag.*, no. 6, pp. 102–112, Nov. 2014.

[6] NGMN Alliance, "5G white paper," Mar. 2015. [Online]. Available: http://www.ngmn.org/5g-white-paper.html

[7] 3GPP TR 22.862, "Feasibility study on new services and markets technology enablers for critical communications; stage 1 (V14.1.0)," Sep. 2016. [Online]. Available: http://www.3gpp.org/DynaReport/22862.htm

[8] 5G-PPP, "5G automotive vision," Oct. 2015. [Online]. Available: https://5g-ppp.eu/wp-content/uploads/2014/02/5G-PPP-White-Paper-on-Automotive-Vertical-Sectors.pdf

[9] J. Medbo, I. Siomina, A. Kangas, and J. Furuskog, "Propagation channel impact on LTE positioning accuracy: A study based on real measurements of observed time difference of arrival," in *Proc. IEEE PIMRC*, Sep. 2009, pp. 2213–2217.

[10] H. Liu, J. Yang, S. Sidhom, Y. Wang, Y. Chen, and F. Ye, "Accurate WiFi based localization for smartphones using peer assistance," *IEEE Trans. Mobile Computing*, vol. 13, no. 10, pp. 2199–2214, Oct. 2014.

[11] D. Dardari, P. Closas, and P. Djuric, "Indoor tracking: Theory, methods, and technologies," *IEEE Trans. Veh. Technol.*, vol. 64, no. 4, pp. 1263–1278, Apr. 2015.

[12] M. Koivisto, M. Costa, J. Werner, K. Heiska, J. Talvitie, K. Leppnen, V. Koivunen, and M. Valkama, "Joint Device Positioning and Clock Synchronization in 5G Ultra-Dense Networks," *IEEE Transactions on Wireless Communications*, vol. 16, no. 5, pp. 2866–2881, May 2017.

[13] W. Yuan, N. Wu, B. Etzlinger, H. Wang, and J. M. Kuang, "Cooperative Joint Localization and Clock Synchronization Based on Gaussian Message Passing in Asynchronous Wireless Networks," *IEEE Transactions on Vehicular Technology*, vol. PP, no. 99, pp. 1–1, 2016.

[14] METIS, "D1.4 Channel models," Feb. 2015. [Online]. Available: https://www.metis2020.com/wp-content/uploads/METIS_D1.4_v3.pdf

[15] H. Kim, X. Ma, and B. Hamilton, "Tracking low-precision clocks with time-varying drifts using Kalman filtering," *IEEE/ACM Trans. Netw.*, vol. 20, no. 1, pp. 257–270, Feb. 2012.

[16] L. F. Auler and R. d'Amore, "Adaptive Kalman Filter for Time Synchronization over Packet-Switched Networks: An Heuristic Approach," in *2007 2nd International Conference on Communication Systems Software and Middleware*, Jan. 2007, pp. 1–7.

[17] A. Bletsas, "Evaluation of Kalman filtering for network time keeping," *IEEE Transactions on Ultrasonics, Ferroelectrics, and Frequency Control*, vol. 52, no. 9, pp. 1452–1460, Sep. 2005.

[18] A. Richter, "Estimation of radio channel parameters: Models and algorithms," Ph.D. dissertation, Ilmenau University of Technology, http://www.db-thueringen.de/servlets/DerivateServlet/Derivate-7407/ilm1-2005000111.pdf, 2005.

[19] S. Särkkä, *Bayesian filtering and smoothing*. Cambridge University Press, 2013.

[20] METIS, "D6.1 Simulation guidelines," Oct. 2013. [Online]. Available: https://www.metis2020.com/wp-content/uploads/deliverables/METIS_D6.1_v1.pdf
[21] P. Kela, J. Turkka, and M. Costa, "Borderless mobility in 5G outdoor ultra-dense networks," *IEEE Access*, vol. 3, pp. 1462–1476, 2015.
[22] R. Akcelik and D. C. Biggs, "Acceleration profile models for vehicles in road traffic," *Transportation Science*, no. 1, pp. 36–54, Feb. 1987.
[23] M. Koivisto, M. Costa, A. Hakkarainen, K. Leppänen, and M. Valkama, "Joint 3D positioning and network synchronization in 5G ultra-dense networks using UKF and EKF," in *Proc. IEEE GLOBECOM Workshops*, Dec. 2016.
[24] S. Fischer, "Observed time difference of arrival (OTDOA) positioning in 3GPP LTE," Jun. 2014. [Online]. Available: https://www.qualcomm.com/media/documents/files/otdoa-positioning-in-3gpp-lte.pdf
[25] P. Mogensen *et al.*, "5G small cell optimized radio design," in *Proc. IEEE GLOBECOM Workshops*, Dec. 2013, pp. 111–116.